Novel polymorphs and polytypes of lithium chloride from structure predictions based on charge equilibration via neural network technique

Samare Rostami,[1,2] S. Alireza Ghasemi,[2] and Stefan Goedecker[3,*]

[1]*The Abdus Salam International Centre for Theoretical Physics, Strada Costiera 11, 34151 Trieste, Italy*

[2]*Department of Physics, Institute for Advanced Studies in Basic Sciences (IASBS), Zanjan 45137-66731, Iran*

[3]*Department of Physics, University of Basel, Klingelbergstrasse 82, Basel 4056, Switzerland*

(Received 10 May 2021; accepted 17 November 2021; published 8 December 2021)

By an extensive structural search using the minima hopping method together with the charge equilibration via neural network technique (CENT) artificial neural network potential, we find several novel lithium chloride structures. Besides reproducing the known low energy phases of LiCl, the structural search reveals 86 new phases of which 42 are energetically lower than the rocksalt phase. We classify our structures based on their structural similarities. While many of them can be considered as polytypes of known structures, there are also entirely unexpected low-density polymorphs that contain empty cages and channels.

DOI: 10.1103/PhysRevMaterials.5.123603

I. INTRODUCTION

Virtually all properties of materials are governed by their crystalline structure. For a given stoichiometry this structure is in general not unique and different polymorphs exist. The prediction of thermodynamically stable crystalline structures by means of computational methods is nowadays a powerful approach in theoretical chemistry and condensed matter physics. To this end, several different computational methods have been developed [1–6] and successfully applied to various types of materials. Lithium halides are known as ionic insulators due to their large band gap and extensive studies have been done to determine the band structures and optical properties of these materials [7–13]. However, in the context of crystal structure prediction, only few studies have been done to discover new phases of lithium halides [14–17]. For decades, only rocksalt (RS) and CsCl phases were known as the most stable phases for all alkali halides at any pressure, and extensive studies have been performed for both phases [18–20]. However, lithium halides behave differently than other alkali halides and can be stabilized in a variety of phases such as wurtzite (WZ) and zinc blende (ZB). Actually, some computational studies predict WZ as a ground state rather than RS at low pressures and temperatures [14,15,21,22].

An extensive exploration of the enthalpy landscape has been performed for 20 binary alkali halide polymorphs by Čančarević *et al.* [14]. They investigated the enthalpies at different pressures at the level of Hartree-Fock and density functional theory (DFT) with six different exchange-correlation functionals. They demonstrated that the energetic ordering of structures varies for different functionals. Results of LiCl indicate that for the BECKE-PWGGA [23], DFT-B3LYP, and BECKE-LYP [24–26] functionals as well as for Hartree-Fock at zero pressure, WZ is energetically the most favorable phase. However, at pressure values of 1.0, 2.0, 2.5, and 2.5 GPa, RS becomes the ground-state structure. In the LDA-PWGGA, LDA-LYP, and LDA-VBH functionals, RS is the putative global minimum for all pressures investigated in their study. In a recent study using the meta-GGA SCAN functional [27], the preference of WZ and RS of lithium halides have been investigated considering the anion size [28]. According to their results, SCAN and Perdew-Burke-Ernzerhof (PBE) functionals both predict WZ as the ground state of LiBr and LiI, but for LiF and LiCl these two functionals are not in agreement. SCAN predicts RS as the ground state whereas PBE predicts WZ.

While the efforts for predicting the theoretical ground state are still going on, Jansen and co-workers found experimental evidence for the existence of WZ phases for lithium halides at low temperatures [15,21,22]. They reported the synthesis of the WZ phase via depositing vapor onto substrates at low temperatures. The proposed temperature windows for the synthesis of WZ structure are 77–273 K for LiI, 173–253 K for LiBr, and 213–243 K for LiCl. They show that LiCl can be synthesized at the above-mentioned temperature in the WZ phase in coexistence with RS and that it transforms at room temperature completely to the RS phase.

In addition to WZ, ZB, and RS one can find a few other polymorphs for LiCl in crystallography databases [29]. A first-principles bottom-up study on nanoclusters and nanocluster-based polymorphs of alkali halides proposed that the zeolite sodalite (SOD) is a stable nanoporous form of LiCl [16]. There are also a few theoretical studies on LiCl nanoclusters [30–32] and monolayer sheets of LiCl [33]. In these works they verify that hexagonal structures are stable and become preferable for large clusters and monolayer sheets.

In this study, we explore the energy landscape of LiCl based on the charge equilibration via neural network technique (CENT) [34]. The validation of our neural network (NN) method for alkali halides is presented in our previous studies on various ionic materials [35]. In this work the

*stefan.goedecker@unibas.ch

NN potential was parametrized for multicomponent systems containing the first three elements of alkali metals and halides. Combining CENT with the minima hopping method (MHM) [5,6,36,37] enables us to explore the energy landscape exhaustively and to find a large variety of new structures. The use of the MHM together with CENT for ionic materials is well established and validated by various studies [38–40].

Here, we report several novel polymorph structures, some of which are identified as polytype groups. Polytypism refers to a class of polymorphs in which the structures have the same periodicity along two axes and vary only along the third axis which is in experiments typically the direction of growth. The best known polytypes belong to the silicon carbide compound family for which over 100 polytypes are reported and a wide range of studies have been done [41–43]. They are grown by a sequence of Si-C bilayer stacks along a direction that generates mixed WZ/ZB phases. While SiC is best known for its polytypism, this phenomenon can also be found in other materials. Polytypism arising from mixing WZ and RS structures can, for instance, be found in MX, where M = Zn, Ga, In and X = S, Se [44–48] and in group III–V compounds like InAs and InSb [49–51]. Moreover, different kinds of polytypism are observed in various ionic materials, for instance, metal dihalides, MX_2 (X = F, Cl, Br, I) [52–54].

II. METHOD

The structural search was performed using the MHM [5,6,36,37] together with the CENT potential. The MHM employs a sequence of short molecular dynamics (MD) trajectories and local geometry optimizations to explore the potential energy surface.

In CENT, the total energy is expressed by the following functional form:

$$U_{\mathrm{tot}}(\{q_i\}) = \sum_{i=1}^{N}\left(E_i^0 + \chi_i q_i + \frac{1}{2}J_{ii}q_i^2\right) + \frac{1}{2}\iint \frac{\rho(\mathbf{r})\rho(\mathbf{r}')}{|\mathbf{r}-\mathbf{r}'|}d\mathbf{r}d\mathbf{r}', \quad (1)$$

where E_i^0 are the energies of the isolated atoms, q_i are the atomic charges, and J_{ii} are the element-dependent atomic hardnesses. χ_i is the environment-dependent electronegativity of atom i, whose functional dependence is given by an artificial neural network (ANN) for each type of atom. The charge density of the system, $\rho(\mathbf{r})$, is considered a superposition of N spherically symmetric Gaussian functions, each centered at the atomic positions $\mathbf{r}_i$ and normalized to the corresponding atomic charges q_i. The q_i in turn depend implicitly on the environment through the atomic electronegativity χ_i, and are obtained by minimizing the total energy of Eq. (1) with respect to q_i. The constraint that the atomic charges have to sum up to the total charge q_{tot}, $\sum_i q_i = q_{\mathrm{tot}}$, has to be taken into account by Lagrange multipliers. We have used a version of the MHM and CENT as implemented in the FLAME package [55].

To generate a database required for training and testing of ANNs, we performed DFT calculations using the PBE [56] exchange-correlation functional within the projector augmented-wave (PAW) [57] formalism as implemented in the Vienna Ab initio Simulation Package (VASP) [58,59]. A plane-wave cutoff energy of 650 eV and dense k-point meshes are chosen to converge the total energies to within 1 meV/atom. The k-point mesh is set by choosing the k-point density to be 0.04 Å^{-1}. The potential was originally trained to the reference structures comprised of different compositions and stoichiometries containing the six elements Li, Na, K, F, Cl, and Br at a fixed oxidation state. The database consisted of the DFT energies and forces of 18 108 bulk configurations [35]. In this study, we employ the same potential without any change.

TABLE I. The lattice constants of lithium chloride (in Å). The values obtained from DFT calculations and CENT are listed together with experimental results reported in Ref. [15] at a temperature of 223 K.

	RS	WZ		
Method	a (Å)	a (Å)	c (Å)	$E_{WZ} - E_{RS}$ (eV)
CENT	5.132	3.855	6.350	−0.024
PBE	5.142	3.921	6.272	−0.025
LDA	4.959	3.795	6.030	0.034
SCAN	5.095	3.881	6.207	0.008
BLYP	5.231	3.964	6.372	−0.069
B3LYP	5.178	3.928	6.299	−0.059
PBEsol	5.064	3.880	6.170	0.015
Expt. (223 K)	5.063	3.852	6.118	

Among the 18 108 structures in the training and validation set of the ANN, 697 are binary structures of LiCl and 3306 structures contain both Li and Cl elements. The root-mean-squared error (RMSE) of the energy and the atomic forces is below 5.5 meV/atom and 70 meV/Å, respectively. A detailed evaluation of this potential for the properties of both binary and ternary structures has been given previously [35].

In order to explore the new structures of lithium chloride, we performed 500 different MHM runs based on the CENT potential with different initial structures from 4 to 32 atoms. Some new high-symmetry structures obtained in the first runs were used as input structures for subsequent runs. For each size, 20 to 40 different runs were performed that generated about 2700 new phases. Out of these, 200 structures were selected with high symmetry and low energy. The dynamic stability of all found structures was tested by computing the phonon spectrum. The phonon frequencies were calculated using the harmonic approach with the nonanalytical term correction as implemented in the PHONOPY package [60]. In this work we present only structures that have nonimaginary phonon frequencies in PBE calculations.

III. RESULTS AND DISCUSSIONS

Besides reproducing all known phases of LiCl reported in the literature, the structural search discovers hundreds of new phases but only high-symmetric structures were further examined. In Table II we report all found dynamically stable structures with space group higher than 20 and energies lower than the RS phase as well as some high-symmetry structures which are energetically at most 42 meV/atom higher than RS. Among all the phases listed in Table II only a few have

TABLE II. Structural data of the new structures. Column 1 and 2 contain our structural label and their space group in the Hermann-Mauguin notation, respectively. In columns 3 and 4 the similarity groups and subgroups according to our classification are listed. Columns 5–10 contain the energies obtained by CENT and PBE and PBE free energies at different temperatures. All energies are reported with respect to the energy of RS phase (C047). In Column 11, the band gaps obtained by the PBE functional are listed. Column 12 contains the coordination numbers of the atoms. If the coordination numbers are different for Li and Cl, both of them are given, followed in parentheses by the number of atoms that have this coordination number. The last column contains the number of atoms in the primitive cell. Asterisks indicate that the structure has previously been reported in the literature. .

				Energy (meV)		Free energy (meV)						
Label	Space group	Group	Subgroup	CENT	PBE	@0 K	@150 K	@300 K	@500 K	Gap (eV)	Coord.	#atom
C001*[a,b]	$P6_3mc$ (186)	G01	SG01	−23	−25	−18	−18	−16	−12	5.95	Li,Cl: 4	4
C002	$R3m$ (160)	G01	SG01	−23	−23	−16	−16	−14	−10	5.96	Li,Cl: 4	6
C003*[a]	$P6_3mc$ (186)	G01	SG01	−23	−23	−15	−16	−13	−9	5.96	Li,Cl: 4	8
C004	$R3m$ (160)	G01	SG01	−23	−23	−15	−16	−13	−9	5.96	Li,Cl: 4	8
C005	$P3m1$ (156)	G01	SG01	−23	−22	−15	−16	−14	−10	5.96	Li,Cl: 4	10
C006	$Pmc2_1$ (26)	G02	SG02	−22	−22	−15	−15	−13	−10	5.91	Li,Cl: 4	24
C007	$P6_3mc$ (186)	G01	SG01	−23	−22	−15	−15	−13	−8	5.96	Li,Cl: 4	12
C008	$Pmn2_1$ (31)	G02	SG02	−21	−21	−14	−14	−13	−9	5.90	Li,Cl: 4	16
C009	$Pbam$ (55)	G02	SG02	−21	−21	−14	−14	−12	−9	5.91	Li,Cl: 4	16
C010*[a]	$F\bar{4}3m$ (216)	G01	SG01	−23	−20	−13	−14	−11	−7	5.97	Li,Cl: 4	2
C011	$Cmc2_1$ (36)	G02	SG02	−20	−19	−12	−13	−11	−8	5.90	Li,Cl: 4	12
C012	$Pnma$ (62)	G02	SG02	−21	−19	−12	−13	−11	−8	5.89	Li,Cl: 4	24
C013	$Pnnm$ (58)	G03	SG05	−15	−19	−12	−12	−11	−8	5.91	Li,Cl: 4	8
C014	$Cmc2_1$ (36)	G02	SG02	−21	−18	−11	−12	−11	−7	5.88	Li,Cl: 4	20
C015	$P3m1$ (156)	G02	SG02	−17	−17	−10	−11	−9	−5	5.85	Li,Cl: 4	16
C016	$Pbca$ (61)	G03	SG05	−21	−17	−10	−11	−10	−6	5.89	Li,Cl: 4	16
C017	$Cmc2_1$ (36)	G02	SG02	−18	−16	−9	−10	−8	−5	5.85	Li,Cl: 4	16
C018	$Imm2$ (44)	G02	SG02	−18	−15	−8	−9	−7	−4	5.90	Li,Cl: 4	18
C019	$Cmc2_1$ (36)	G03	SG05	−18	−13	−6	−7	−6	−3	5.85	Li,Cl: 4	12
C020	$Pmn2_1$ (31)	G03	SG05	−13	−11	−4	−5	−3	−1	5.80	Li,Cl: 4	16
C021	$P\bar{3}m1$ (164)	G04	SG08	−14	−10	−3	−5	−3	−1	5.80	Li,Cl: 4	16
C022	$Cmcm$ (63)	G04	SG07	−16	−9	−3	−4	−2	1	5.86	Li,Cl: 4	12
C023	$Imm2$ (44)	G04	SG07	−18	−9	−2	−3	−1	3	5.91	Li,Cl: 4	22
C024	$Iba2$ (45)	G02	SG02	−7	−8	−1	−2	−0	3	5.84	Li,Cl: 4	16
C025	$Pmc2_1$ (26)	G02	SG02	−13	−7	−0	−1	0	4	5.77	Li,Cl: 4	16
C026	$Pbcn$ (60)	G03	SG06	−12	−7	0	−1	0	3	5.82	Li,Cl: 4	16
C027	$Pnma$ (62)	G03	SG06	−16	−6	1	−0	1	4	5.80	Li,Cl: 4	8
C028	$Ama2$ (40)	G02	SG02	−11	−6	1	0	1	4	5.80	Li,Cl: 4	16
C029	$Pmn2_1$ (31)	G04	SG07	−16	−5	2	1	2	5	5.89	Li,Cl: 4	16
C030	$P6_3/m$ (176)	G03	SG06	−13	−5	2	0	1	3	5.92	Li,Cl: 4	12
C031	$Cmc2_1$ (36)	G04	SG08	−6	−5	2	1	2	4	5.72	Li,Cl: 4	12
C032	$Pnma$ (62)	G04	SG07	−17	−5	2	1	3	6	5.91	Li,Cl: 4	16
C033	$P31m$ (157)	G04	SG08	−11	−5	2	1	2	4	5.71	Li,Cl: 4	12
C034*[c]	$P6_3/mmc$ (194)	G08	SG12	11	−4	−1	−2	−3	−3	5.59	Li,Cl: 5	4
C035	$Pmc2_1$ (26)	G02	SG02	−12	−3	3	2	3	6	5.79	Li,Cl: 4	16
C036	$Imm2$ (44)	G04	SG07	−15	−3	4	3	4	7	5.89	Li,Cl: 4	14
C037	$Pnma$ (62)	G03	SG06	−13	−3	4	2	3	5	5.87	Li,Cl: 4	16
C038	$Imm2$ (44)	G04	SG07	−15	−3	4	3	5	8	5.90	Li,Cl: 4	14
C039	$Aem2$ (39)	G02	SG02	−2	−2	4	3	4	7	5.81	Li,Cl: 4	12
C040	$Immm$ (71)	G04	SG08	−13	−2	5	4	5	8	5.86	Li,Cl: 4	16
C041	$Imm2$ (44)	G04	SG07	−10	−2	5	4	6	9	5.87	Li,Cl: 4	14
C042	$P3_1$ (144)	G02	SG04	−5	−2	5	4	6	9	5.89	Li,Cl: 4	18
C043	$Pmn2_1$ (31)	G04	SG07	−14	−1	6	5	6	9	5.90	Li,Cl: 4	12
C044	$F222$ (22)	G03	SG06	−6	−0	6	5	6	8	5.81	Li,Cl: 4	16
C045	$I4/m$ (87)	G03	SG06	−4	−0	6	5	5	7	5.90	Li,Cl: 4	8
C046	$Pmmn$ (59)	G04	SG07	−14	−0	7	6	7	10	5.90	Li,Cl: 4	12
C047*[d]	$Fm\bar{3}m$ (225)	G06	SG10	0	0	−0	0	0	0	6.29	Li,Cl: 6	2
C048	$Pmm2$ (25)	G04	SG07	−9	1	8	7	9	12	5.88	Li,Cl: 4	12
C049	$Amm2$ (38)			0	2	8	7	7	10	5.51	Li,Cl: 4(6),5(1)	14
C050	$I4cm$ (108)	G02	SG03	21	2	9	8	9	11	5.78	Li,Cl: 4	8

TABLE II. (*Continued.*)

Label	Space group	Group	Subgroup	Energy (meV)		Free energy (meV)				Gap (eV)	Coord.	#atom
				CENT	PBE	@0 K	@150 K	@300 K	@500 K			
C051	*Imm*2 (44)	G04	SG07	−12	2	9	8	9	12	5.89	Li,Cl: 4	10
C052	*C*222 (21)	G04	SG08	−8	4	11	11	12	16	5.74	Li,Cl: 4	20
C053	*Imm*2 (44)	G04	SG07	−7	5	12	11	12	15	5.89	Li,Cl: 4	10
C054	*Cmm*2 (35)	G04	SG08	−8	6	13	12	13	16	5.85	Li,Cl: 4	16
C055*[e]	$Pm\bar{3}n$ (223)	G09	SG13	16	7	13	11	10	10	5.37	Li,Cl: 4	12
C056	*Ibam* (72)	G08	SG12	6	8	10	9	9	9	5.53	Li,Cl: 5	16
C057	$P6_3/mmc$ (194)	G06	SG10	10	8	8	8	9	10	6.24	Li,Cl: 6	8
C058	$R\bar{3}$ (148)	G02	SG03	6	8	14	13	13	15	5.90	Li,Cl: 4	12
C059	*P*6*cc* (184)	G02	SG03	19	8	14	13	14	16	5.95	Li,Cl: 4	24
C060	*Pmm*2 (25)	G04	SG07	−5	8	15	14	15	17	5.87	Li,Cl: 4	16
C061	$P6_3mc$ (186)	G05	SG09	−7	10	16	15	17	19	5.61	Li,Cl: 4	8
C062	$R\bar{3}m$ (166)	G05	SG09	−7	10	16	15	17	19	5.62	Li,Cl: 4	8
C063	$P\bar{6}m2$ (187)	G06	SG10	15	10	11	11	12	13	6.23	Li,Cl: 6	12
C064	$I\bar{4}m2$ (119)	G07	SG11	−8	11	17	16	17	20	5.40	Li,Cl: 4	10
C065	$Pmn2_1$ (31)	G04	SG07	−4	11	18	16	17	20	5.90	Li,Cl: 4	16
C066	*Pmm*2 (25)	G04	SG07	−4	11	18	17	18	20	5.88	Li,Cl: 4	8
C067	$P\bar{3}c1$ (165)	G03	SG06	11	12	18	16	17	18	5.96	Li,Cl: 4	24
C068	*Cmmm* (65)	G03	SG05	10	13	19	18	18	21	5.23	Li,Cl: 4	14
C069	$P3_121$ (152)	G02	SG04	9	14	20	19	20	23	5.83	Li,Cl: 4	6
C070	$P3_221$ (154)	G02	SG04	9	14	20	19	20	23	5.83	Li,Cl: 4	6
C071	*Cmme* (67)	G08	SG12	7	15	17	16	17	18	5.77	Li,Cl: 5	12
C072	*Imma* (74)	G08	SG12	13	15	17	16	16	16	5.52	Li,Cl: 5	20
C073*[a]	$P6_3/mmc$ (194)	G06	SG10	25	15	16	17	18	19	6.25	Li,Cl: 6	4
C074	*Imm*2 (44)	G04	SG07	−2	15	22	21	21	24	5.86	Li,Cl: 4	14
C075	*Imm*2 (44)	G04	SG07	0	16	23	21	21	23	5.82	Li,Cl: 4	6
C076	$R\bar{3}$ (148)			15	16	23	20	20	20	5.95	Li,Cl: 4	12
C077	$I\bar{4}$ (82)	G04	SG08	−1	17	23	22	23	25	5.87	Li,Cl: 4	10
C078	$P4_2/mmc$ (131)	G07	SG11	−5	18	24	23	24	26	5.40	Li,Cl: 4	8
C079	$P\bar{4}m2$ (115)	G07	SG11	−2	18	24	23	24	26	5.39	Li,Cl: 4	8
C080	$F\bar{4}3m$ (216)	G09	SG13	20	18	25	22	22	23	5.48	Li,Cl: 4	10
C081	$P6/mcc$ (192)	G08	SG12	24	18	21	20	20	20	5.76	Li,Cl: 5	24
C082	*Amm*2 (38)			23	20	25	23	21	21	5.54	Li,Cl: 3(1),4(6),5(1)	16
C083	*Amm*2 (38)			18	20	23	23	23	24	5.76	Li,Cl: 4(1),5(2)	6
C084	*Pmm*2 (25)	G04	SG07	−0	21	28	26	26	27	5.86	Li,Cl: 4	6
C085	$Pmn2_1$ (31)	G06	SG10	−6	22	25	24	24	24	5.79	Li: 4(4),6(4) Cl: 4(2),5(4),6(2)	16
C086	*Amm*2 (38)	G06	SG10	21	24	26	25	25	26	5.96	Li: 4(2),6(4) Cl: 5(4),6(2)	12
C087	*Amm*2 (38)	G09	SG13	14	27	33	29	27	25	5.59	Li,Cl: 3(1),4(4)	10
C088	*Pmmm* (47)	G09	SG13	37	27	32	30	28	28	5.05	Li,Cl: 4	24
C089	$I\bar{4}m2$ (119)	G07	SG11	4	29	35	34	35	37	5.39	Li,Cl: 4	6
C090	$P3m1$ (156)	G09	SG13	25	38	44	40	38	36	5.40	Li,Cl: 3(1),4(4)	10
C091	*I*4 (79)			24	40	44	42	40	38	5.73	Li,Cl: 4(4),5(1)	10
C092	*Imm*2 (44)	G09	SG13	42	40	46	43	42	42	5.11	Li,Cl: 4	16
C093	$P\bar{4}3m$ (215)			77	42	50	49	51	54	5.97	Li,Cl: 4	8

[a]Reference [62].
[b]Reference [15].
[c]Reference [35].
[d]Reference [18].
[e]Reference [16].

previously been reported. These are indicated by an asterisk. The remaining 86 structures are novel. Atomic positions and phonon dispersion of all structures are presented in the Supplemental Material [61].

Except for RS, the well-studied phase for all alkali halides, and WZ, which can be synthesized at low temperatures and pressures for lithium halides, there are no other experimentally reported structures. As discussed in the Introduction,

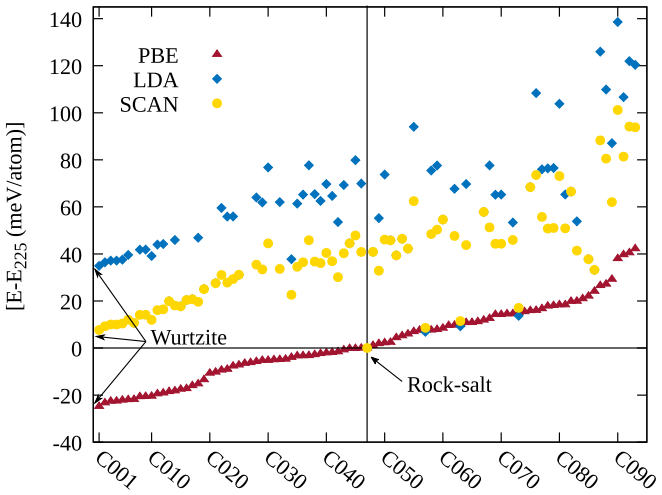

FIG. 1. Comparison of the relative energies of our structures calculated by the LDA, SCAN, and PBE functionals with respect to RS energy. During relaxation with LDA and SCAN, some of the structures transform to other phases; therefore, their energies are excluded.

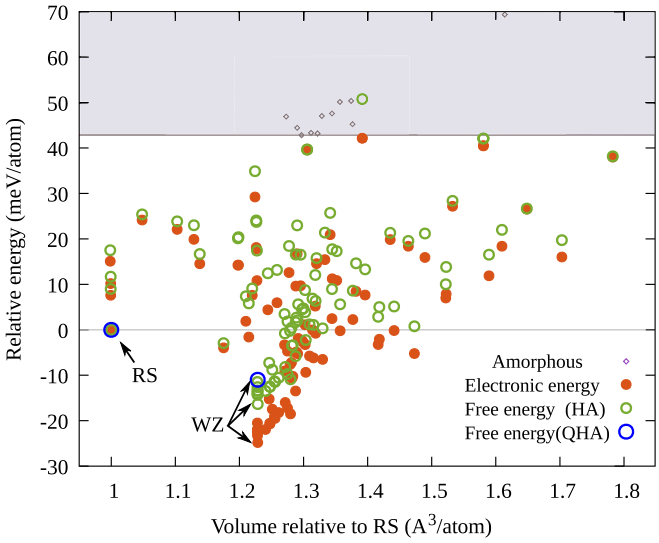

FIG. 2. Energies and free energies at temperature 300K of all found structures with respect to the rock salt phase of LiCl vs their relative volume (Vol/Vol_{RS}). The plot indicates that the most of structures have a lower density than RS and are close to the WZ phase. The gray region and points show the domain of the amorphous structures.

the energetic ordering of lithium halide phases depends on the DFT functionals used. The influence of the functional on structural properties and energies is illustrated in Table I. PBEsol and SCAN give lattice constants that are closer to the experimental ones than other methods and in both of them RS is lower in energy than WZ. LDA underestimates the cell parameters and predicts RS as the ground state. Other functionals overestimate the lattice parameters and predict WZ to be lower in energy than RS. Since our CENT potential was generated by a reference database trained with the PBE functional, its results follow the PBE trends. In SCAN, which is considered a reliable functional for ionic systems, the energy of RS is only 8 meV/atom lower than WZ and, as reported in Ref. [28] for the larger cation sizes found in LiBr and LiI, WZ is the generally accepted global minimum. However, the experimental studies confirm the existence of WZ as a metastable phase of LiCl. Our calculations in this work are based on PBE since it is the quasistandard for crystal structures in crystallography databases [29,62].

In Fig. 1 the formation energies of all PBE, SCAN, and LDA relaxed structures are shown. Some LDA and SCAN points are removed because during optimization the structures were not stable and transformed into other phases. The numbering of structures is chosen according to their energetic ordering in PBE. As shown, RS, which is the global minimum of LDA and SCAN, is at position 47 in the PBE energetic ordering. The LDA, SCAN, and PBE energies do in general not correlate very well as can be seen from Fig. 1.

In Table II, formation energies of all structures obtained by PBE and CENT are listed together with the free energies at different temperatures (0, 150, 300, and 500 K). Our free energies are computed via PHONOPY [60] based on the phonon frequencies in the harmonic approximation. Increasing temperature reduces the PBE energy difference between the RS- and WZ-type structures but the effect is not strong enough to reverse the energetic ordering. In Table II we also compare the band gaps. With a gap of 6.29 eV, RS has the largest gap. The smallest one, 5.05 eV, belongs to C088 which is a low-density structure with capsulelike holes inside (see Fig. 11).

In Fig. 2, the relative potential and free energies at 300 K of all studied structures are plotted against relative volume (Vol/Vol_{RS}). Both potential and free energies are reported with respect to the RS phase. The scatterplot shows that except for three structures (C057, C063, and C073) which are structurally similar to the RS phase, others have a lower density than RS and most of them have volumes close to the WZ phase.

Recently a criterion was proposed to estimate the chances for a material to be synthesized [63]. According to this criterion a polymorph can in general be synthesized if its energy is lower than the energy of the amorphous phase. We have therefore selected 260 amorphous configurations from the trajectories of NVT MD simulations at a temperature of 1500 K which is about 600 K above the LiCl melting point. Ten different MD simulations were run employing cubic cells containing 108 atoms in random positions with volume/atom 10–100 % larger than rocksalt phases. The structures were selected every 10 ps after 10 ps equilibrium time and then both the cell and atomic positions were relaxed. Finally, 11 amorphous configurations with the lowest energy in different volumes were relaxed by PBE. In Fig. 2, the domain of these amorphous structures is shown by a gray region. Since the energy of all the amorphous structures is well above the energy of our crystalline polymorphs we can conclude that all our structures might be synthesized. All found structures are relaxed at different pressures (from 0 to 2.0 GPa) and their enthalpies are shown in Table I of the Supplemental Material [61]. Some of the structures are not stable during relaxation at higher pressures and transform to other phases. In this case a blank can be found in the table. The result indicates that

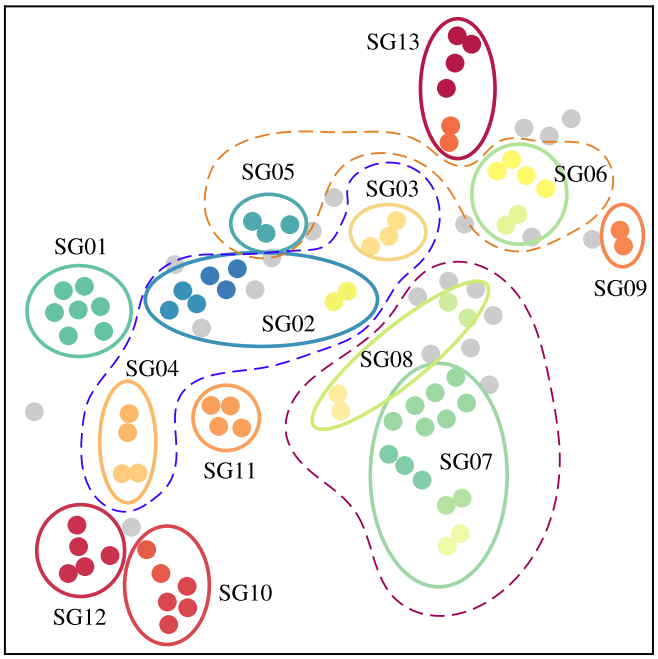

FIG. 3. Clusters of structures obtained with the HDBSCAN method. Structures belonging to the same subgroups are shown in identical colors and encircled with dashed lines. The full lines encircle the subgroups obtained by merging the results of the HDBSCAN and the advanced-density-peaks clustering methods.

for pressures of more than 1 GPa, RS becomes the preferred phase of LiCl.

Crystallographic classification

Many of our structures are actually combinations of other more elementary structures or modifications of other structures. This is particularly true if we have large unit cells. Many of the structures can be considered polytypes. The variations mostly consist of a rotation or translation along a symmetry axis, an elimination of a line or plane of crystal sites, or combinations thereof. In general, classifying and distinguishing the structures is difficult and ambiguous.

To classify our structures, we employ two different clustering methods, the HDBSCAN as implemented in the clustering library of PYTHON [64] and the advanced-density-peaks method of Rodriguez and Laio as implemented in an open source code [65]. Since the grouping results depend on the algorithms and their parameters, comparing and merging the results of these two different methods helps us to classify the structure in a more reliable way (see Fig. 3).

We characterize our structures by the overlap matrix fingerprint [66]. In this way nine different main group of configurations were detected which contain at least two members. Three of these groups can be subdivided into smaller subgroups by changing the criteria. So, in total we define 13 subgroups of polytypes. We list these similarity groups and subgroups in Table II and depict eight of these subgroups in Figs 4–11. As illustrated in the figures, each

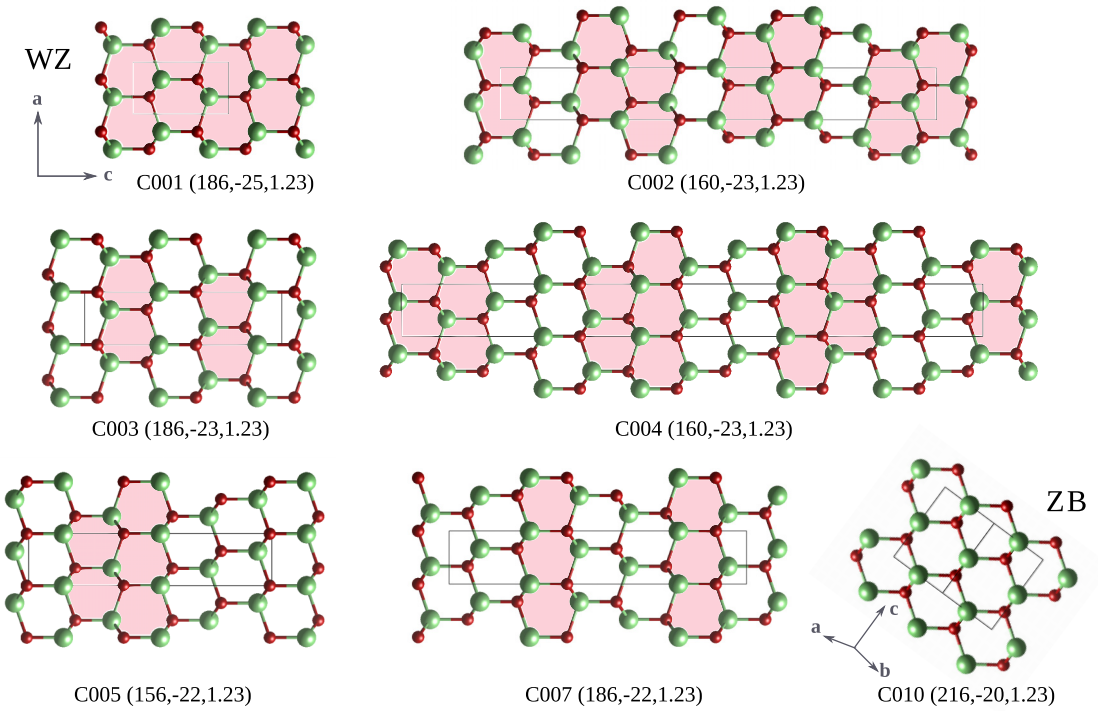

FIG. 4. Subgroup 1. The first structure of this group, C001, is the WZ which is the global minimum and the last one, C010, belongs to ZB. The numbers in parentheses are the space group number, the energy difference with respect to rocksalt, and the volume with respect to rocksalt V/V_{RS}. In all structures, green and red spheres correspond to Li and Cl elements respectively and the boxes indicate the crystalline cells. Identical polygons are indicated by coloring.

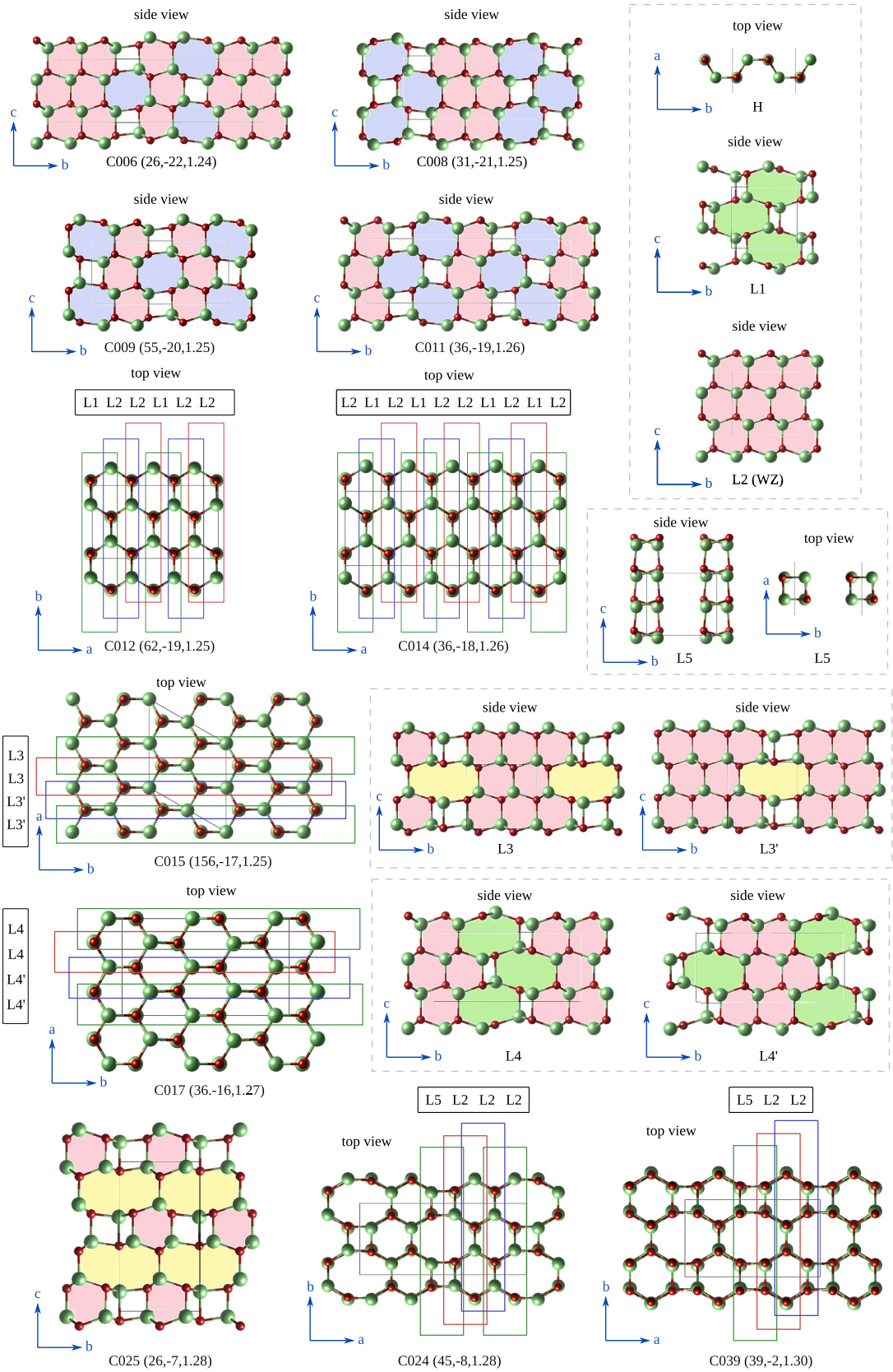

FIG. 5. Subgroup 2. Because of the complexity of structures in this subgroup, we analyze the similarities by cutting the lattice into different building block layers. All structures except C006, C008, C009, C011, and C025 are constructed by a sequence of different building block layers which are also shown. The boxes in the main structures give the top view of the different building layers, and the colors (red, green, and blue) are used to distinguish different layers. The side views of these building block layers are shown in dashed boxes labeled L1–L5, where the superscript prime indicates a translation of this layer. Otherwise the same conventions are used as in Fig. 4.

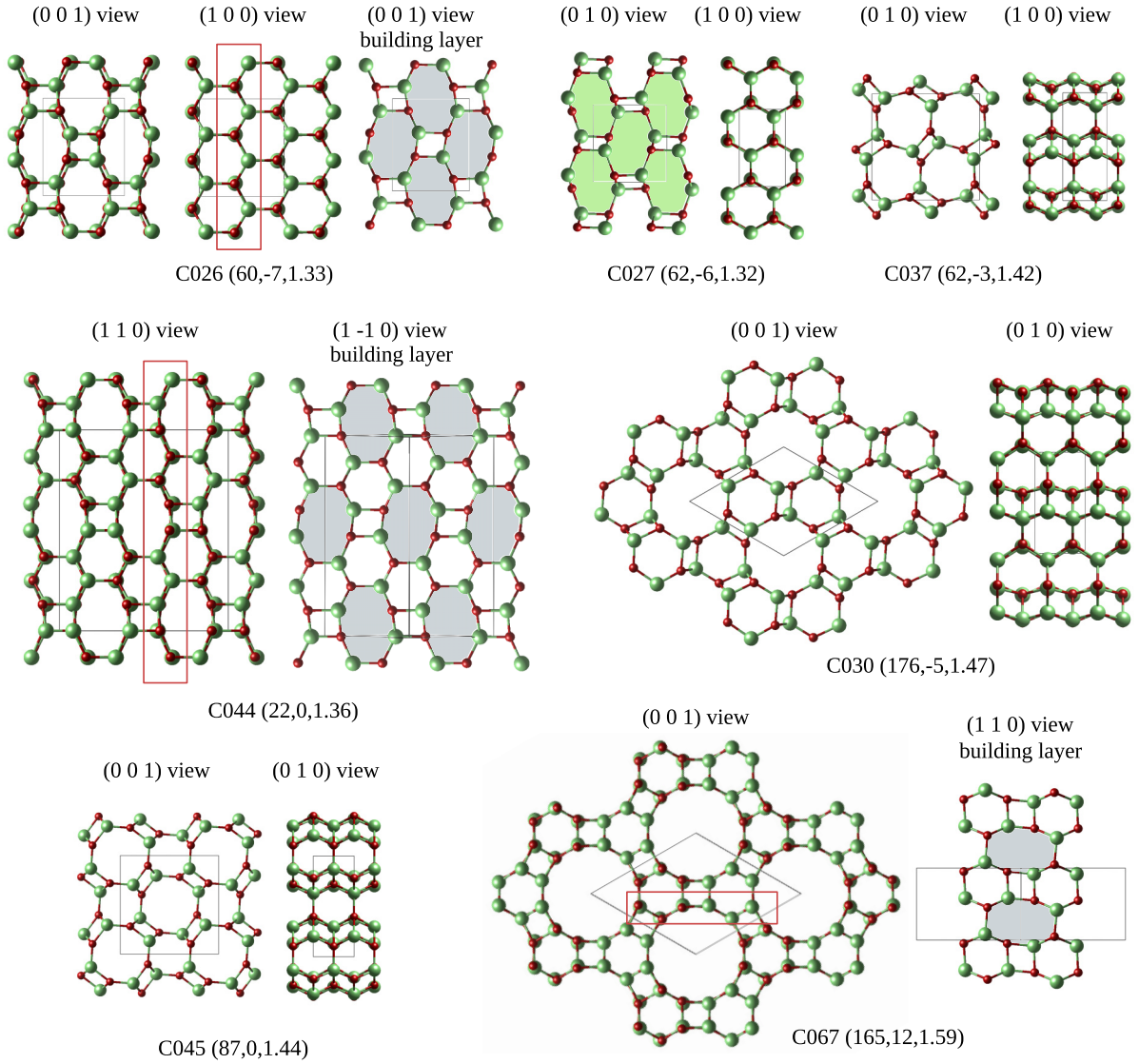

FIG. 6. Subgroup 06. Red boxes indicate the building block layers of the lattice and the black boxes the crystalline cell. The same conventions are used as in Fig. 4.

group is obtained by different stacking patterns along different directions.

The first group with one subgroup of polytype phases contains the known structures of WZ and ZB. By sorting the structures with respect to their energies, we can indicate that this group starts from our global minimum WZ(C001) and ends at ZB(C010) as illustrated in Fig. 4. The protocol for generating the configurations of this group, C002–C005 and C007, starts from the WZ, extends the lattice along c axes, and then applies a sequence of rotations in different layers by $\pm 60^{\circ}$ along the c axis. Our first classification of LiCl crystals is similar to the well-known polytypes of silicon carbide which are formed by the stacking sequence of SiC layers [41–43]. Group 2 is made from 20 phases in three subgroups. The structures of subgroup 2 in this group are shown in Fig. 5. To illustrate the pattern of structures in a better way, we separate the constructions into different building block layers and list the stacking sequence of each structure. In this group C009 is similar to the Z-carbon structure [67]. Configurations of group 3 are very similar to the ones in group 2. One of the two subgroups of these classifications is shown in Fig. 6. Subgroup 7 from group 4 contains 18 polytypes and is in this way the most densely populated group. Some of the structures are shown in Fig. 7. Starting from ZB and performing rotations around the (110) axes followed by a translation along the 110 axis can generate other structures in this group. The interpretation of these configurations is not unique and depends upon the points of view. For example, from crystallography, we could say that for most of these structures we have mirror symmetry or a combination of it by a transition along the mirror axes. These rearrangements reduce the density of the generated structures' configuration. Subgroup 10 contains configurations that are related to the rocksalt structure. C057, C063,

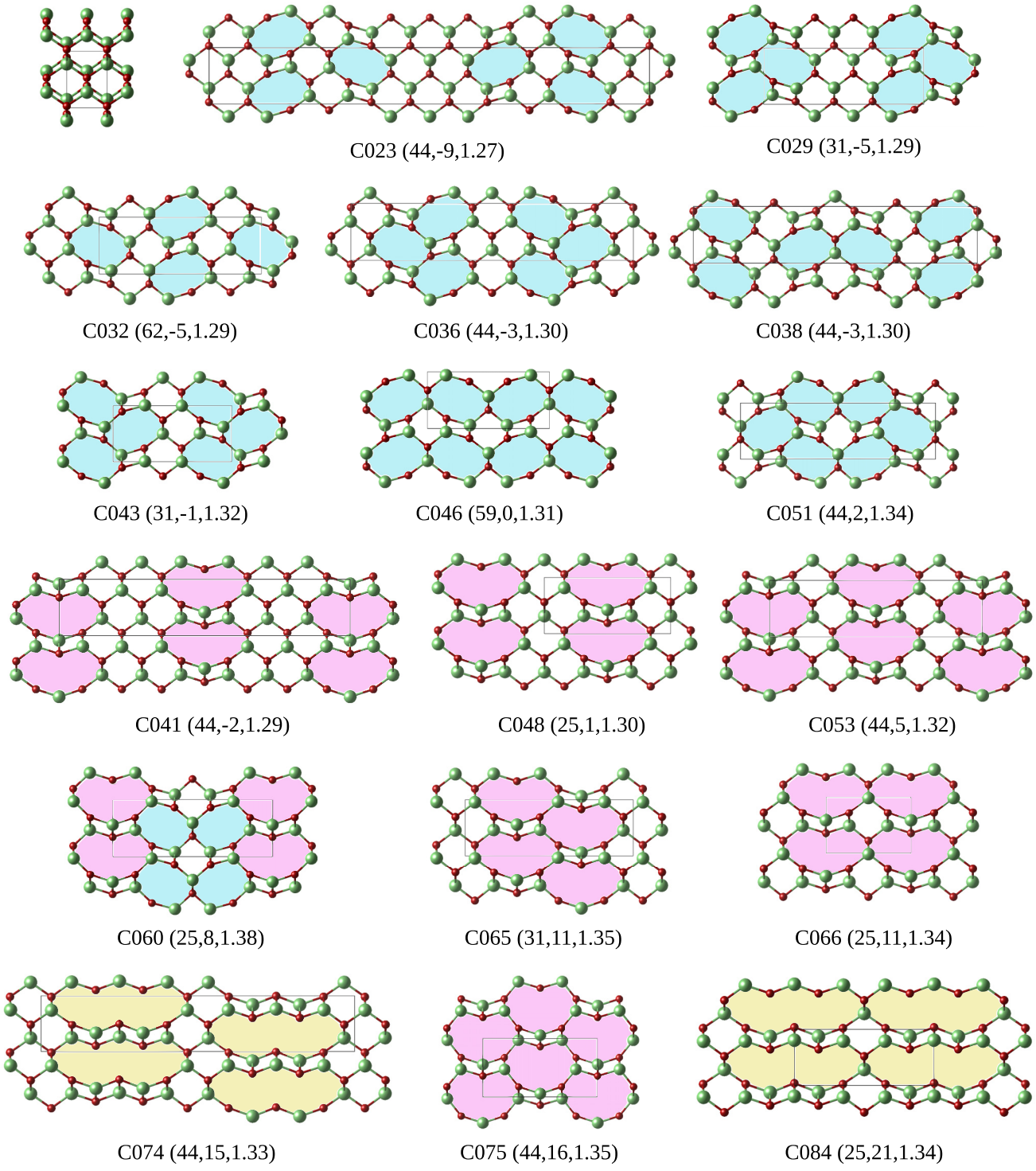

FIG. 7. Subgroup 07. The area of the colored polygons in this subgroup is increasing which results in a continuous lowering of the density. The same conventions are used as in Fig. 4.

and C073 can be derived from the rocksalt structure (C047) by rotating or flipping planes along a certain direction shown by the dashed line in Fig. 8. The two remaining configurations of this subgroup are also similar to the other members. Structures in subgroup 11 are formed by a combination of rotations and translations along the *c* axis starting from ZB (Fig. 9).

The initial structure of subgroup 12, first introduced in Ref. [35], is graphitelike (see Fig. 10), and taking out stripes of atoms in the graphitic plane gives the low-density structure C081 with a space group of 192. All these group members have the same coordination number 5 for all atoms.

Finally, the low-density configurations which belong to subgroup 13 are presented in Fig. 11. Four structures of this

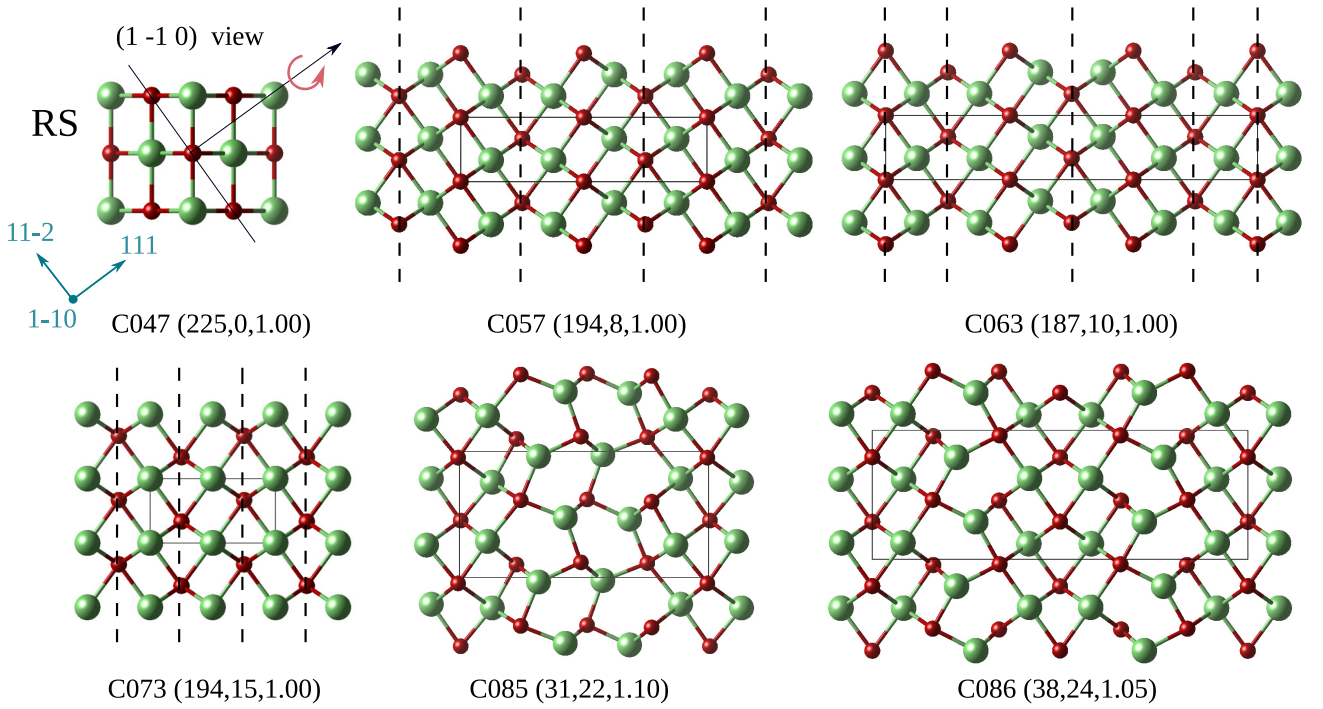

FIG. 8. Subgroup 10 contains the structures derived from rocksalt by 180° rotations of one or several planes around the 111 axis. The same conventions are used as in Fig. 4.

group (C055, C080, C088, and C092) are built by cagelike building blocks. C090 in this group has the lowest density among all of our structures.

In the majority of groups, the coordination number of both Li and Cl is 4, as listed in Table II. The exceptions occur in structures of subgroups 10 and 12 with coordination numbers 5 and 6, respectively, as well as low-density structures in group 13 with the coordination number 3.

In Fig. 12 the x-ray diffraction (XRD) patterns of nine polymorphs are plotted by employing the VESTA visualization code [68]. The similarity of structures in each group is clear by overlapping the intensities in different angles.

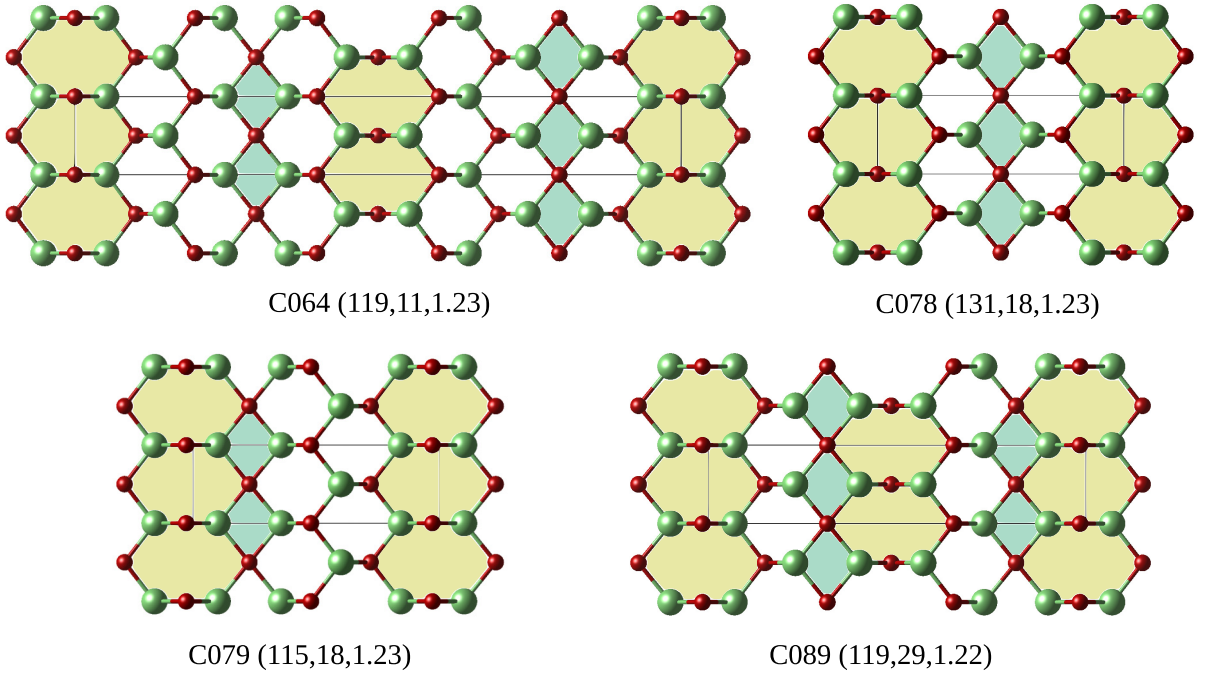

FIG. 9. Subgroup 11. The structures in this subgroup are constructed by a combination of rotations and translations along the *c* axis of ZB that preserve the density of ZB. The same conventions are used as in Fig. 4.

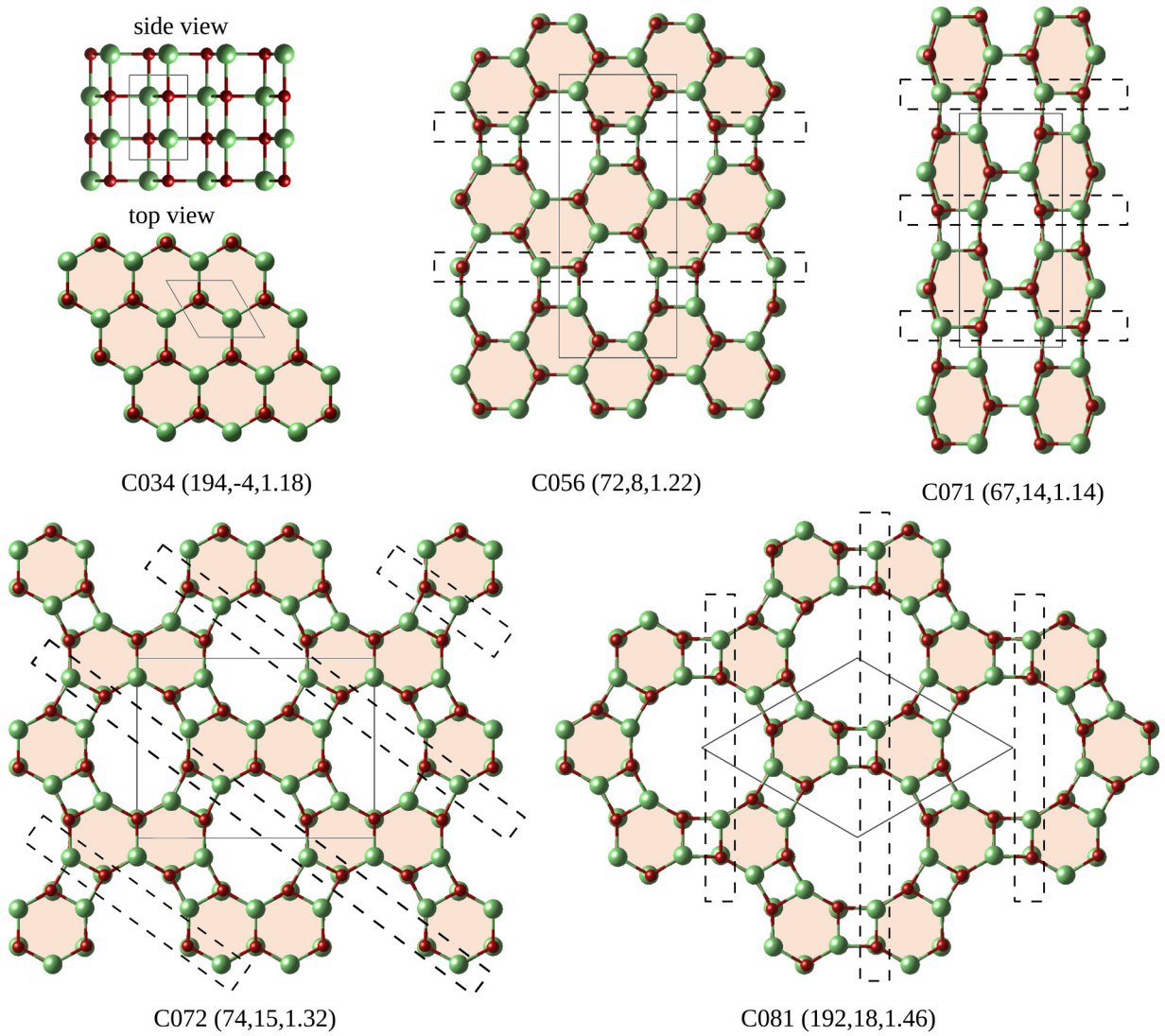

FIG. 10. Subgroup 12. All these structures share a similar side view in which the atoms are in parallel planes. The sequence of structures C081, C072, C056, and C034 in this subgroup is obtained by cutting out the stripes framed by the dashed lines and then relaxing the structures. In the same way structure C034 can be obtained from structure C071. The same conventions are used as in Fig. 4.

IV. CONCLUSIONS

Based on an efficient structure prediction method, minima hopping, together with a fast neural network potential, we are able to explore the potential energy surface of LiCl exhaustively. In addition to the well-known structures, we find 86 new structures of LiCl. Even though the present state of the art of DFT is not accurate enough to predict the exact energetic ordering of these structures, they are all quite low in energy and might therefore be synthesized. Synthesizing low-density structures is challenging. Nevertheless, this has been achieved, for instance, for silicon by growing the material in the presence of helium atoms and then extracting the helium [69]. RS-type structures can increase their stability faster with increasing temperature than other structures. In order to cope with the large structural diversity, we classify our structures into groups and subgroups consisting mainly of polytypes. Among our novel structures are amazing low-density structures that contain large empty channels and cages. Those empty regions might be filled by molecules to obtain ionic materials with new functionalities that could be used for various applications such as gas separation for which up to now other low-density materials such as zeolites are used [70–73]. The structures that we found are also candidate structures for other lithium halides.

ACKNOWLEDGMENTS

Computational resources were provided by the Swiss National Supercomputing Center (CSCS) in Lugano under the projects s707 and s963. Calculations were also performed at the sciCORE scientific computing core facility at the University of Basel [74].

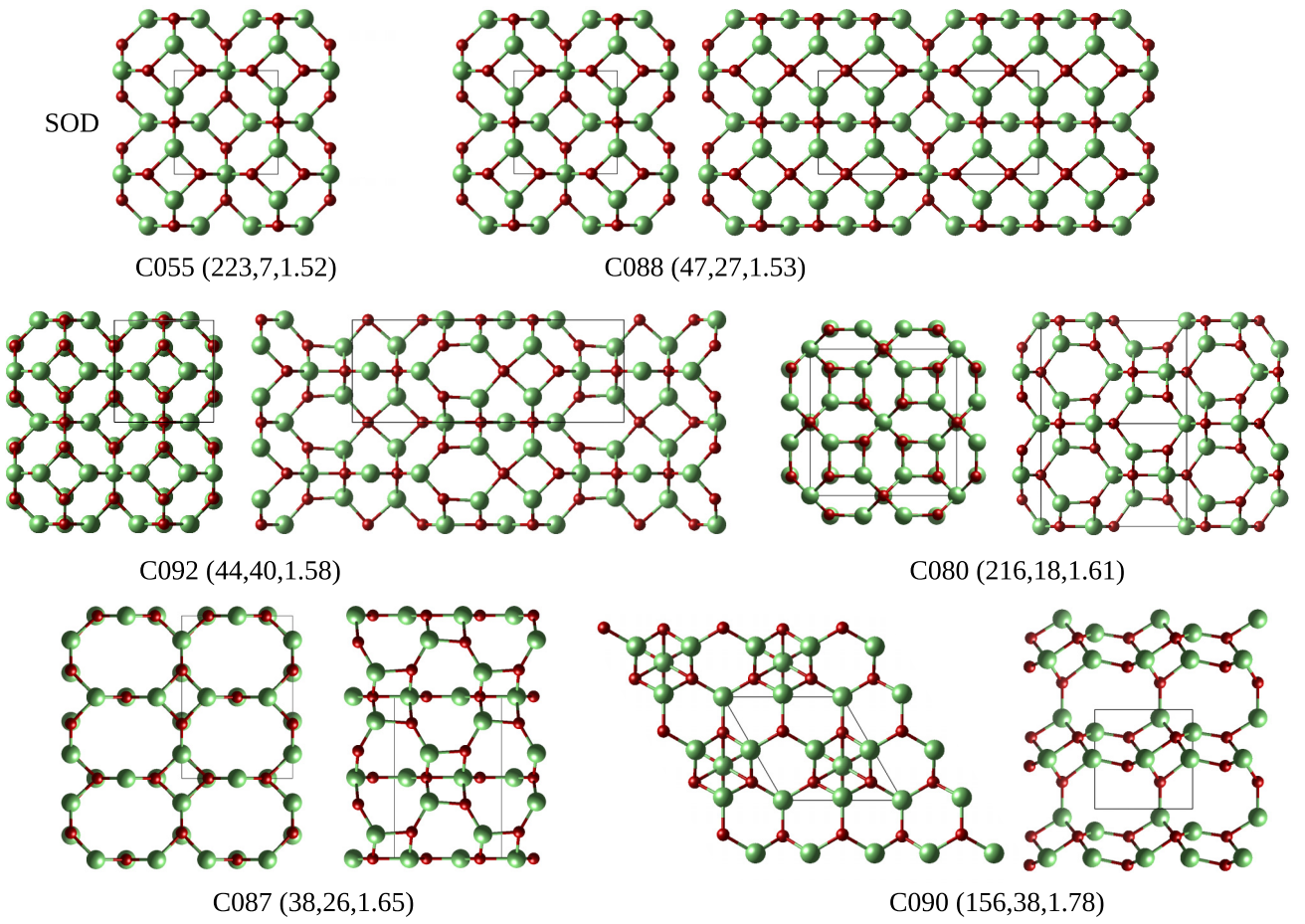

FIG. 11. Subgroup 13. This group contains the low-density structures. Structures C055, C080, C088, and C092 have a low density because they contain cages, whereas the other structures are low density because of empty channels. The same conventions are used as in Fig. 4.

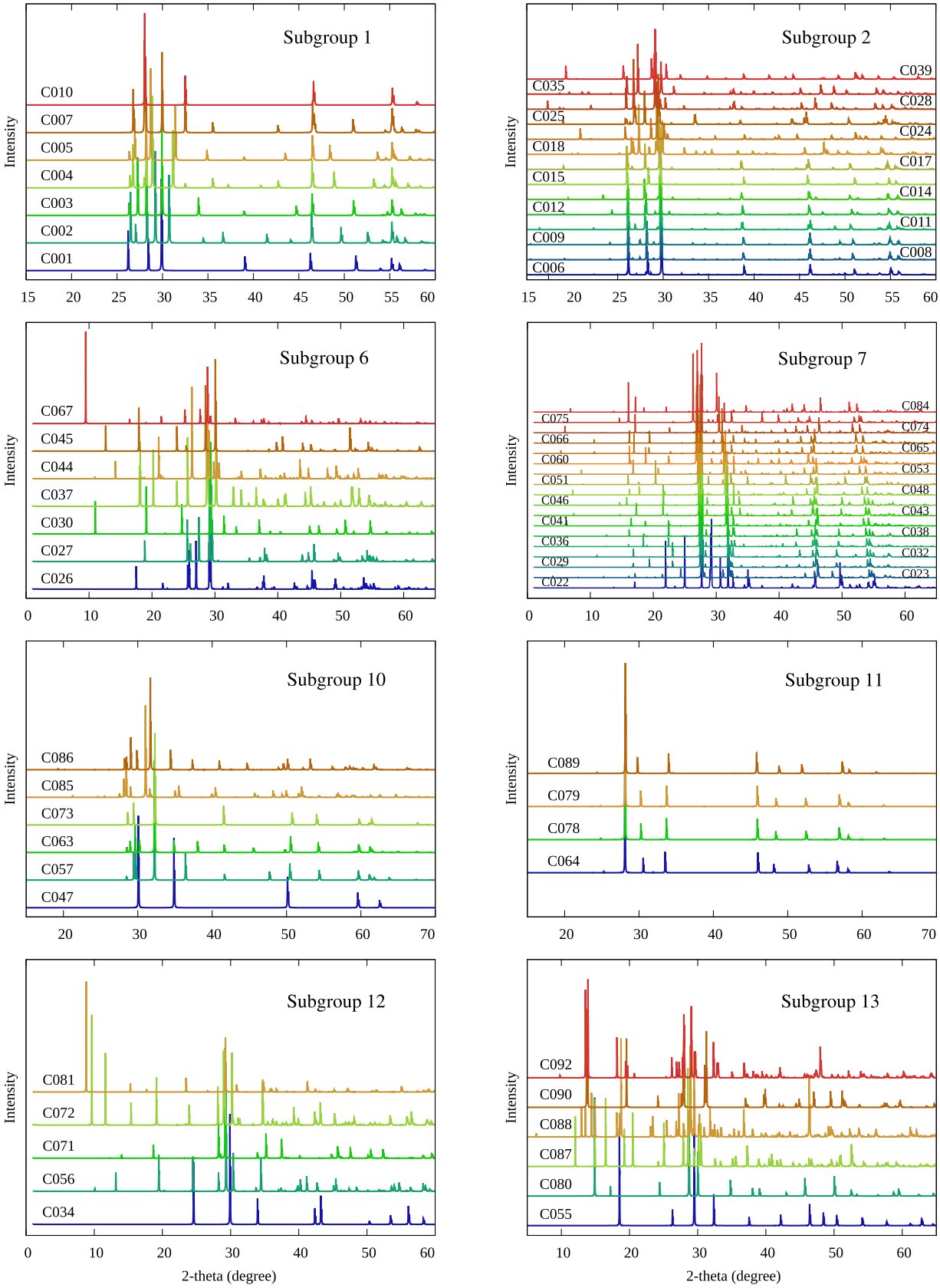

FIG. 12. The x-ray diffraction pattern for polytype subgroups.

[1] D. J. Wales and J. P. K. Doye, J. Phys. Chem. A **101**, 5111 (1997).
[2] A. R. Oganov and C. W. Glass, J. Chem. Phys. **124**, 244704 (2006).
[3] C. J. Pickard and R. J. Needs, J. Phys.: Condens. Matter **23**, 053201 (2011).
[4] Y. Wang, J. Lv, L. Zhu, and Y. Ma, Phys. Rev. B **82**, 094116 (2010).
[5] S. Goedecker, J. Chem. Phys. **120**, 9911 (2004).
[6] M. Amsler and S. Goedecker, J. Chem. Phys. **133**, 224104 (2010).
[7] Y.-F. Jiang, N.-P. Wang, and M. Rohlfing, J. Chem. Phys. **139**, 214710 (2013).
[8] C. R. Gopikrishnan, D. Jose, and A. Datta, AIP Adv. **2**, 012131 (2012).
[9] A. M. Pendás, V. Luaña, J. M. Recio, M. Flórez, E. Francisco, M. A. Blanco, and L. N. Kantorovich, Phys. Rev. B **49**, 3066 (1994).
[10] S. Iwata, S. Ishii, and K. Ohno, Mater. Trans. **46**, 1100 (2005).
[11] M. Kiguchi, G. Yoshikawa, S. Ikeda, and K. Saiki, Phys. Rev. B **71**, 153401 (2005).
[12] A. B. Kunz, Phys. Rev. **175**, 1147 (1968).
[13] L. I. Johansson and S. B. M. Hagström, Phys. Scr. **14**, 55 (1976).
[14] Ž. Čančarević, J. Schön, and M. Jansen, Chem. Asian J. **3**, 561 (2008).
[15] A. Bach, D. Fischer, and M. Jansen, Z. Anorg. Allg. Chem. **635**, 2406 (2009).
[16] W. Sangthong, J. Limtrakul, F. Illas, and S. T. Bromley, J. Mater. Chem. **18**, 5871 (2008).
[17] A. Aguado, A. Ayuela, J. M. López, and J. A. Alonso, Phys. Rev. B **56**, 15353 (1997).
[18] D. B. Sirdeshmukh, L. Sirdeshmukh, and K. G. Subhadra, *Alkali Halides* (Springer, Berlin, 2001).
[19] B. Erdinc, M. N. Secuk, M. Aycibin, S. E. Gülebagan, E. K. Dogan, and H. Akkus, Comput. Condens. Matter **4**, 6 (2015).
[20] M. Prencipe, A. Zupan, R. Dovesi, E. Aprà, and V. R. Saunders, Phys. Rev. B **51**, 3391 (1995).
[21] D. Fischer, A. Moller, and M. Jansen, Z. Anorg. Allg. Chem. **630**, 2697 (2004).
[22] Y. Liebold-Ribeiro, D. Fischer, and M. Jansen, Angew. Chem. Int. Ed. **47**, 4428 (2008).
[23] J. P. Perdew and Y. Wang, Phys. Rev. B **45**, 13244 (1992).
[24] A. D. Becke, Phys. Rev. A **38**, 3098 (1988).
[25] A. D. Becke, J. Chem. Phys. **98**, 5648 (1993).
[26] C. Lee, W. Yang, and R. G. Parr, Phys. Rev. B **37**, 785 (1988).
[27] J. Sun, A. Ruzsinszky, and J. P. Perdew, Phys. Rev. Lett. **115**, 036402 (2015).
[28] J. H. Yang, D. A. Kitchaev, and G. Ceder, Phys. Rev. B **100**, 035132 (2019).
[29] A. Jain, S. P. Ong, G. Hautier, W. Chen, W. D. Richards, S. Dacek, S. Cholia, D. Gunter, D. Skinner, G. Ceder, and K. A. Persson, APL Mater. **1**, 011002 (2013).
[30] T. Croteau and G. N. Patey, J. Chem. Phys. **124**, 244506 (2006).
[31] P. C. Rodrigues and F. M. S. Fernandes, Eur. Phys. J. D **44**, 109 (2007).
[32] P. C. Rodrigues and F. M. S. Fernandes, J. Mol. Struct.: THEOCHEM **946**, 94 (2010).
[33] D. Hoat, M. Naseri, N. T. Binh, J. Rivas-Silva, T. V. Vu, and G. H. Cocoletzi, Phys. E **123**, 114168 (2020).
[34] S. A. Ghasemi, A. Hofstetter, S. Saha, and S. Goedecker, Phys. Rev. B **92**, 045131 (2015).
[35] S. Rostami, M. Amsler, and S. A. Ghasemi, J. Chem. Phys. **149**, 124106 (2018).
[36] M. Sicher, S. Mohr, and S. Goedecker, J. Chem. Phys. **134**, 044106 (2011).
[37] S. Roy, S. Goedecker, and V. Hellmann, Phys. Rev. E **77**, 056707 (2008).
[38] E. R. Khajehpasha, S. Goedecker, and S. A. Ghasemi, J. Comput. Chem. **42**, 699 (2021).
[39] R. Rasoulkhani, H. Tahmasbi, S. A. Ghasemi, S. Faraji, S. Rostami, and M. Amsler, Phys. Rev. B **96**, 064108 (2017).
[40] S. Rostami, N. Seriani, S. A. Ghasemi, and R. Gebauer, Phys. Rev. Mater. **5**, 063605 (2021).
[41] S. Nakashima and M. Hangyo, Solid State Commun. **80**, 21 (1991).
[42] R. Cheung, *Silicon Carbide Microelectromechanical Systems for Harsh Environments* (Imperial College Press, London, 2006).
[43] H. Matsunami, in *Encyclopedia of Materials: Science and Technology* (Elsevier, Amsterdam, 2001), pp. 1192–1197.
[44] J. Srour, M. Badawi, F. E. H. Hassan, and A. Postnikov, J. Chem. Phys. **149**, 054106 (2018).
[45] F. Boutaiba, A. Belabbes, M. Ferhat, and F. Bechstedt, Phys. Rev. B **89**, 245308 (2014).
[46] B. Zvyagin, Comput. Math. Appl. **16**, 569 (1988).
[47] S. Mardix, Bull. Mineral. **109**, 131 (1986).
[48] S. J. Magorrian, V. Zólyomi, and N. D. Drummond, Phys. Rev. B **103**, 094118 (2021).
[49] D. Kriegner, C. Panse, B. Mandl, K. A. Dick, M. Keplinger, J. M. Persson, P. Caroff, D. Ercolani, L. Sorba, F. Bechstedt, J. Stangl, and G. Bauer, Nano Lett. **11**, 1483 (2011).
[50] F. Bechstedt and A. Belabbes, J. Phys.: Condens. Matter **25**, 273201 (2013).
[51] N. Benyahia, A. Zaoui, D. Madouri, and M. Ferhat, J. Appl. Phys. **121**, 125701 (2017).
[52] P. A. Beckmann, Cryst. Res. Technol. **45**, 455 (2010).
[53] A. Grzelak, J. Gawraczyński, T. Jaroń, D. Kurzydłowski, A. Budzianowski, Z. Mazej, P. J. Leszczyński, V. B. Prakapenka, M. Derzsi, V. V. Struzhkin, and W. Grochala, Inorg. Chem. **56**, 14651 (2017).
[54] M. Derzsi, A. Grzelak, P. Kondratiuk, K. Tokár, and W. Grochala, Crystals **9**, 423 (2019).
[55] M. Amsler, S. Rostami, H. Tahmasbi, E. R. Khajehpasha, S. Faraji, R. Rasoulkhani, and S. A. Ghasemi, Comput. Phys. Commun. **256**, 107415 (2020).
[56] J. P. Perdew, K. Burke, and M. Ernzerhof, Phys. Rev. Lett. **77**, 3865 (1996).
[57] P. E. Blöchl, Phys. Rev. B **50**, 17953 (1994).
[58] G. Kresse and J. Furthmüller, Comput. Mater. Sci. **6**, 15 (1996).
[59] G. Kresse and J. Furthmüller, Phys. Rev. B **54**, 11169 (1996).
[60] A. Togo and I. Tanaka, Scr. Mater. **108**, 1 (2015).
[61] See Supplemental Material at http://link.aps.org/supplemental/10.1103/PhysRevMaterials.5.123603 for structural data and phonon dispersion of all crystals discussed here.
[62] S. Kirklin, J. E. Saal, B. Meredig, A. Thompson, J. W. Doak, M. Aykol, S. Rühl, and C. Wolverton, npj Comput. Mater. **1**, 15010 (2015).
[63] M. Aykol, S. S. Dwaraknath, W. Sun, and K. A. Persson, Sci. Adv. **4**, eaaq0148 (2018).

[64] L. McInnes, J. Healy, and S. Astels, J. Open Source Software **2**, 205 (2017).
[65] A. Rodriguez and A. Laio, Science **344**, 1492 (2014).
[66] L. Zhu, M. Amsler, T. Fuhrer, B. Schaefer, S. Faraji, S. Rostami, S. A. Ghasemi, A. Sadeghi, M. Grauzinyte, C. Wolverton, and S. Goedecker, J. Chem. Phys. **144**, 034203 (2016).
[67] M. Amsler, J. A. Flores-Livas, L. Lehtovaara, F. Balima, S. A. Ghasemi, D. Machon, S. Pailhès, A. Willand, D. Caliste, S. Botti, A. San Miguel, S. Goedecker, and M. A. L. Marques, Phys. Rev. Lett. **108**, 065501 (2012).
[68] K. Momma and F. Izumi, J. Appl. Crystallogr. **41**, 653 (2008).
[69] S. Ding, J. Shi, J. Xie, W. Cui, P. Zhang, K. Yang, J. Hao, L. Zhang, and Y. Li, npj Comput. Mater. **7**, 89 (2021).
[70] D. Xu, H. Lv, and B. Liu, Front. Chem. **6**, 550 (2018).
[71] R. Martinez-Franco, M. Moliner, Y. Yun, J. Sun, W. Wan, X. Zou, and A. Corma, Proc. Natl. Acad. Sci. USA **110**, 3749 (2013).
[72] N. Kosinov, J. Gascon, F. Kapteijn, and E. J. Hensen, J. Membr. Sci. **499**, 65 (2016).
[73] N. Togashi, K. Sugiyama, J. Yu, S. Qiu, and O. Terasaki, Solid State Sci. **13**, 684 (2011).
[74] http://scicore.unibas.ch/.